Performance Evaluation of Improved Fast PMIPv6-Based Network Mobility for Intelligent Transportation Systems

Seonggeun Ryu, Ji-Woong Choi, and Kyung-Joon Park

Abstract: **The network mobility basic support (NEMO BS) protocol has been investigated to provide Internet connectivity for a group of nodes, which is suitable for intelligent transportation systems (ITS) applications. NEMO BS often increases the traffic load and handover latency because it is designed on the basis of mobile Internet protocol version 6 (MIPv6). Therefore, schemes combining proxy MIPv6 with NEMO (P-NEMO) have emerged to solve these problems. However, these schemes still suffer from packet loss and long handover latency during handover. Fast P-NEMO (FP-NEMO) has emerged to prevent these problems. Although the FP-NEMO accelerates handover, it can cause a serious tunneling burden between the mobile access gateways (MAGs) during handover. This problem becomes more critical as the traffic between the MAGs increases. Therefore, we propose a scheme for designing an improved FP-NEMO (IFP-NEMO) to eliminate the tunneling burden by registering a new address in advance. When the registration is completed before the layer 2 handover, the packets are forwarded to the new MAG directly and thereby the IFP-NEMO avoids the use of the tunnel between the MAGs during handover. For the evaluation of the performance of the IFP-NEMO compared with the FP-NEMO, we develop an analytical framework for fast handovers on the basis of P-NEMO. Finally, we demonstrate that the IFP-NEMO outperforms the FP-NEMO through numerical results.**

Index Terms: **Fast handovers, intelligent transportation systems (ITS), mobility management, network mobility (NEMO), performance analysis, proxy mobile Internet protocol version 6 (PMIPv6).**

I. INTRODUCTION

Intelligent transportation systems (ITS) have attracted considerable interest in recent years. Although ITS applications were initially designed for safety-oriented communications, the role of infotainment has rapidly become significant [1]. In other words, Internet access service for ITS applications is required. For maintaining a vehicle's Internet connectivity for a group of nodes moving together, network mobility basic support (NEMO BS) [2] was developed by the Internet engineering task force (IETF). NEMO BS is considered in the ITS standards because it is a protocol that is able to provide NEMO [3], [4]. The international organization for standardization (ISO) TC204 WG16 has developed communications access for land mobiles (CALM), which uses NEMO BS referred to as the ITS station reference architecture [5]. The European telecommunications standards institute (ETSI) has standardized geographic addressing and routing (GeoNetworking) initially specified by the GeoNet European project, and NEMO BS has been combined with GeoNetworking [4], [6], [7].

NEMO BS, a mobility support protocol uniquely designed to manage the mobility of a moving network, ensures session continuity for all the nodes in a mobile network. In NEMO, a unique device called a mobile router (MR) is defined to extend the mobile node (MN) of mobile Internet protocol version 6 (MIPv6) [8] by adding a capability routing between its point of attachment and a subnet that moves with the MR. For instance, the MR handles communication with a fixed infrastructure and provides access to the passengers' devices using a convenient short-range radio technology in transportation systems. Thus, the MR supports mobility for mobile network nodes (MNNs) attached to it, thereby enabling the MNNs not to recognize their movements.

Although NEMO BS seems to fit well in the context of ITS, it has several problems. One of the problems is that NEMO BS does not incorporate route optimization (RO) with which MNNs can directly communicate with the correspondent nodes (CNs). There have been many schemes to carry out RO in various NEMO environments [9]–[16]. These schemes enable the MNNs to directly communicate with their CNs in various scenarios. In this paper, we do not consider RO for NEMO.

In addition to the RO problem, the more critical problem of NEMO BS is that NEMO BS incurs packet loss and long handover latency during handover. Proxy MIPv6 (PMIPv6) [17] has been adopted in NEMO [18]–[20] to solve these problems. PMIPv6 was developed to perform network-based mobility management. This approach does not require the MN to be involved in the exchange of the handover signaling messages between itself and the home agent (HA). A mobile access gateway (MAG) serves as a proxy mobility agent in the network by performing mobility management on behalf of the MN attached to the network. Thus, PMIPv6-based NEMO (P-NEMO) enhances the handover performance of the NEMO. Fig. 1 shows the architectural overview of the P-NEMO. When the MR moves to a new MAG (NMAG), the NMAG performs proxy registration on behalf of the MR to maintain the connectivity to the Internet. The proxy registration consists of a proxy binding update (PBU) and proxy biding acknowledgement (PBA) messages. The PBU and PBA messages are exchanged between the

Manuscript received September 15, 2012.

K.-J. Park is the corresponding author.

This work was supported in part by the National Research Foundation (NRF) funded by the Ministry of Education, Science and Technology (MEST) of Korea (2010-0022076, 2012R1A1A1009742), and in part by the DGIST R&D Program funded by the MEST of Korea (13-BD-04).

The authors are with the Department of Information and Communication Engineering, Daegu Gyungbuk Institute of Science and Technology (DGIST), Daegu, Republic of Korea, email: {sgryu, jwchoi, kjp}@dgist.ac.kr.

Digital Object Identifier 10.1109/JCN.2013.000027

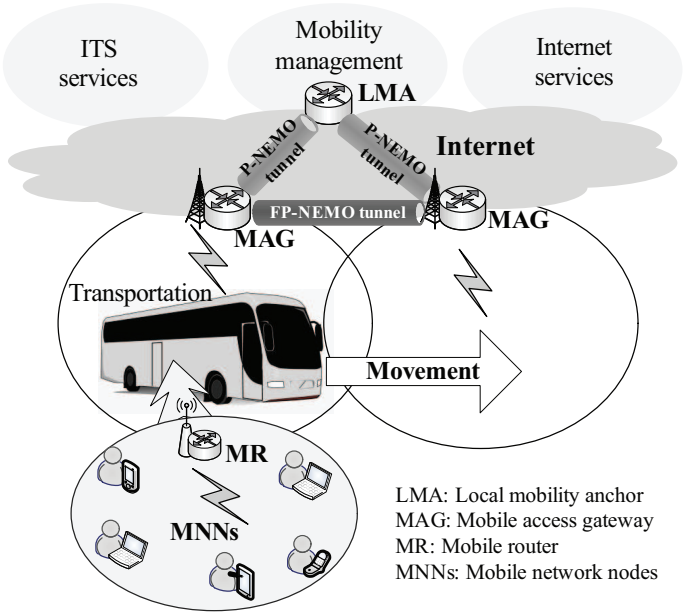

Fig. 1. Architectural overview of PMIPv6-based NEMO.

NMAG and a local mobility anchor (LMA), which is the HA for the MR in the PMIPv6 domain. However, the P-NEMO still suffers from packet loss during handover. Fast P-NEMO (FP-NEMO) was introduced by Lee *et al.* [4] to prevent the packet loss and reduce the handover latency. FP-NEMO uses wireless layer 2 events to anticipate the impending handover. A tunnel is established between a previous MAG (PMAG) and an NMAG to prevent packet loss during handover. The packets destined for MNNs are forwarded to the NMAG during handover.

Even though the FP-NEMO accelerates the handover procedure through tunneling, it can cause a serious tunneling burden between the MAGs. This is because all the packets destined for the MNNs are forwarded to the NMAG through the tunnel between the PMAG and the NMAG. This problem becomes more critical when there already exists heavy traffic between the MAGs. For example, when many MNNs are communicating with the CNs and the link between the PMAG and the NMAG is congested, the tunnel that is established during handover is overloaded. Hence, the packets traversing the tunnel are lost.

In this paper, we propose a scheme for designing an improved FP-NEMO (IFP-NEMO) to eliminate the tunneling burden. The IFP-NEMO adopts a tentative binding update (TBU) scheme [21], [22], which performs the registration to the HA prior to the layer 2 handover. When the registration is completed, the packets are directly forwarded to the NMAG and thereby the IFP-NEMO avoids the tunnel utilization between the PMAG and the NMAG during handover. Furthermore, the IFP-NEMO reduces the handover latency of the FP-NEMO because the registration is performed in advance. This study is a significant extension of our preliminary work [23] by considering all the aspects of FP-NEMO and IFP-NEMO, such as the predictive mode, reactive mode, and handover latency. We describe the detailed handover operation of the IFP-NEMO. We define both the predictive and the reactive modes of the IFP-NEMO, while the FP-NEMO is assumed to operate only in the predictive mode. Further, both IFP-NEMO and FP-NEMO are analyzed through an analytical framework for fast handovers on the basis of the P-NEMO. The analytical framework consists of mobility modeling, costs analysis, and handover latency analysis. In the analytical framework, the two modes of fast handover are considered, whereas in the previous studies, only the predictive mode was considered to evaluate the handover performance.

The main contributions of this paper are as follows: First, we point out the significant tunneling burden of the FP-NEMO by investigating the fast handover schemes with NEMO. This problem was not considered in the previous studies. Second, we propose an IFP-NEMO to eliminate the tunneling burden of the FP-NEMO by performing the registration in advance. In addition to mitigating the tunneling burden, the IFP-NEMO reduces the handover latency. Third, we develop a detailed analytical framework to evaluate the IFP-NEMO performance as compared with that of the FP-NEMO.

The rest of this paper is organized as follows. As a prelimi nary, Section II describes the NEMO, P-NEMO, and FP-NEMO. In Section III, we present the proposed scheme for designing an IFP-NEMO. Sections IV and V present the analytical framework and numerical results, respectively. Finally, Section VI concludes the paper.

II. PRELIMINARY

Internet access in vehicles is necessary for supporting various ITS applications. Although MIPv6 can support mobility in a vehicle, it results in many signaling messages when a large number of MNNs in the vehicle simultaneously move. For reducing the signaling burden of all the nodes in the vehicle, NEMO BS was introduced, which supports network mobility in the vehicular networks. NEMO BS is an efficient and scalable scheme, because mobility management is transparent to all the nodes in the vehicle. In other words, MNNs do not transmit and receive signaling messages during handover because the MR provides mobility for all the MNNs connected to it. When the MR moves to a new network, it generates a care-of address (CoA) and transmits a binding update (BU) message to inform about its new location to the HA. The HA further transmits a binding acknowledgement (BA) message back to the MR. Further, a bidirectional tunnel between the MR and the HA is established and all the packets destined for the MNNs attached to the MR are delivered through this tunnel.

NEMO BS is suitable for ITS applications; however, it introduces packet loss and long handover latency during handover. This is because the handover procedure of NEMO BS is based on that of MIPv6. Schemes combining NEMO and PMIPv6 (P-NEMO) were presented in [18]–[20] to solve these problems. PMIPv6 was intended to provide network-based IP mobility management support to the MNs without requiring the participation of the MNs in any IP mobility related signaling. The mobility entities in the network track the movements of the MNs and initiate mobility signaling and set up the required routing state. The core mobility entities are the LMA and the MAG; the former is responsible for maintaining the MN reachability state as the HA does, and the latter is the entity that per-

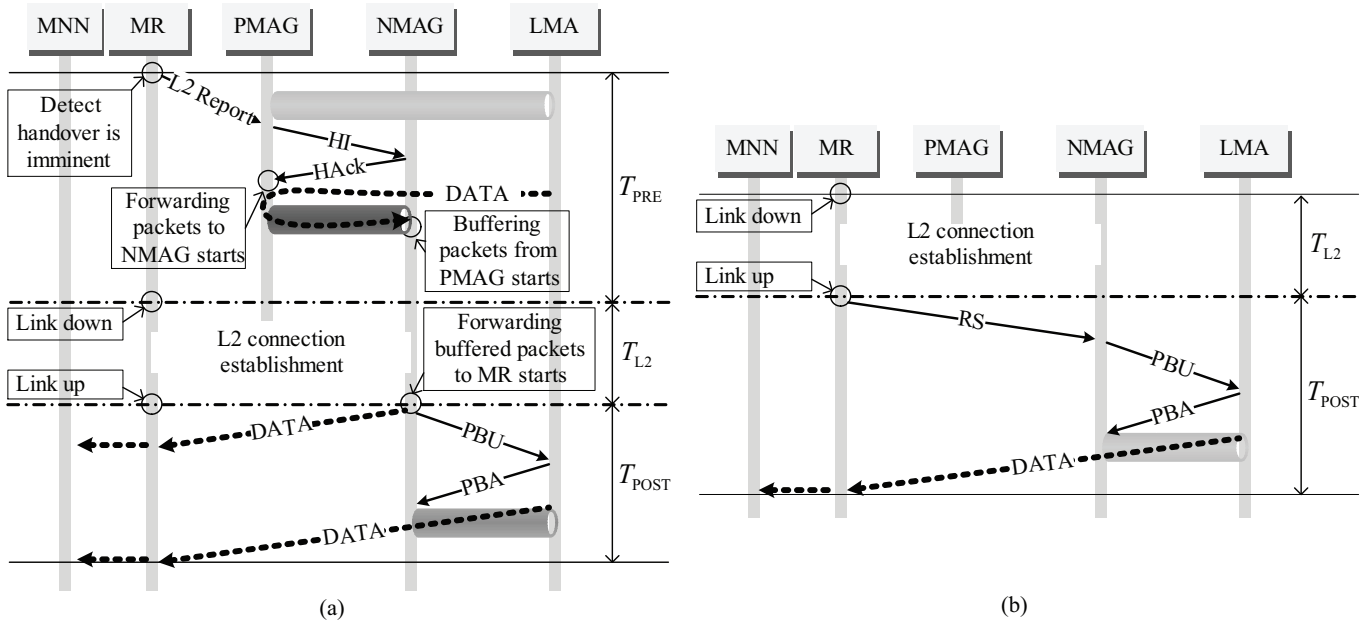

Fig. 2. Handover operation of FP-NEMO: (a) The predictive mode and (b) the reactive mode.

forms the mobility management on behalf of the MNs. In the P-NEMO, the MAG manages the mobility of the MR. Thus, handover signaling induced by the MR is mitigated and the handover latency is reduced.

However, the P-NEMO still causes packet loss, because all the packets destined for the MR are lost during handover. FP-NEMO has emerged as an extension to the P-NEMO [4] to solve these problems. The FP-NEMO can reduce the packet loss and the handover latency of the P-NEMO by adopting fast handovers for PMIPv6 (FPMIPv6) [24]. FP-NEMO uses wireless layer 2 events to anticipate the impending handover of the vehicle's MR. Further, a tunnel is established between the MAGs prior to the attachment of the MR to the NMAG. Thus, the packets are forwarded to the NMAG, without loss during handover.

Fig. 2 illustrates the detailed handover operations of the FP-NEMO. The operation of the FP-NEMO is divided into the predictive mode and the reactive mode because there are two modes of operation in FPMIPv6. In the predictive mode of the FP-NEMO, a bidirectional tunnel between the PMAG and NMAG is established prior to the attachment of the MR to the NMAG. As shown in Fig. 2(a), when the MR detects that a handover is imminent, it reports its movement to the PMAG. On receiving the report, the PMAG transmits a handover initiate (HI) message to the NMAG. The HI message includes the MN ID, home network prefix (HNP), and the address of the LMA that is currently serving the MR. The NMAG transmits a handover acknowledge (HAck) message back to the PMAG. When the PMAG receives the HAck message, a tunnel is established between the PMAG and the NMAG, and thereby, the packets destined for the MNNs are forwarded to the NMAG through this tunnel. These packets are buffered at the NMAG. The buffered packets are forwarded to the MR, after the MR attaches to the NMAG. Further, the NMAG updates the binding cache entry (BCE) in the LMA for the MR by transmitting a PBU message. When the NMAG receives the PBA message, handover is completed. Fig. 2(b) shows the reactive mode of the FP-NEMO. The reactive mode of the FP-NEMO operates as the general P-NEMO does, because it was not defined in [4].

III. SCHEME FOR DESIGNING IMPROVED FAST PMIPV6-BASED NEMO

In the FP-NEMO, the characteristics of the NEMO were not fully examined, although the FP-NEMO reduced the packet loss and handover latency by using tunneling. For example, many MNNs connected to the MR in the NEMO simultaneouly move, which can cause serious performance degradation due to the tunneling burden during handover. Tunneling increases the traffic burden on the link between the PMAG and the NMAG. When many MNNs transmit or receive data packets in high traffic density, the tunnel is particularly overloaded, causing serious congestion.

Therefore, an IFP-NEMO is proposed in this paper to eliminate the tunneling burden and to reduce the handover latency. The IFP-NEMO adopts the tentative binding update scheme [21], [22], which registers the MR to the HA prior to the layer 2 handover. Before the layer 2 handover is begun, a tentative PBU message (TPBU) is transmitted to the LMA to register the new CoA in advance. Further, the LMA directly forwards the packets destined for the MMNs to the NMAG. As a result, the IFP-NEMO avoids using the tunnel between the MAGs during handover, and thereby, the packets destined for the MNNs are delivered through various paths between the LMA and the NMAG. In addition, the handover latency is reduced because the registration to the LMA is performed beforehand. Therefore, the IFP-NEMO is a suitable solution for the P-NEMO in ITS.

The operation of the IFP-NEMO is divided into the predictive mode and the reactive mode because the IFP-NEMO operation follows the fast handovers in the P-NEMO. Fig. 3 shows the detailed handover operation of the IFP-NEMO. The oper-

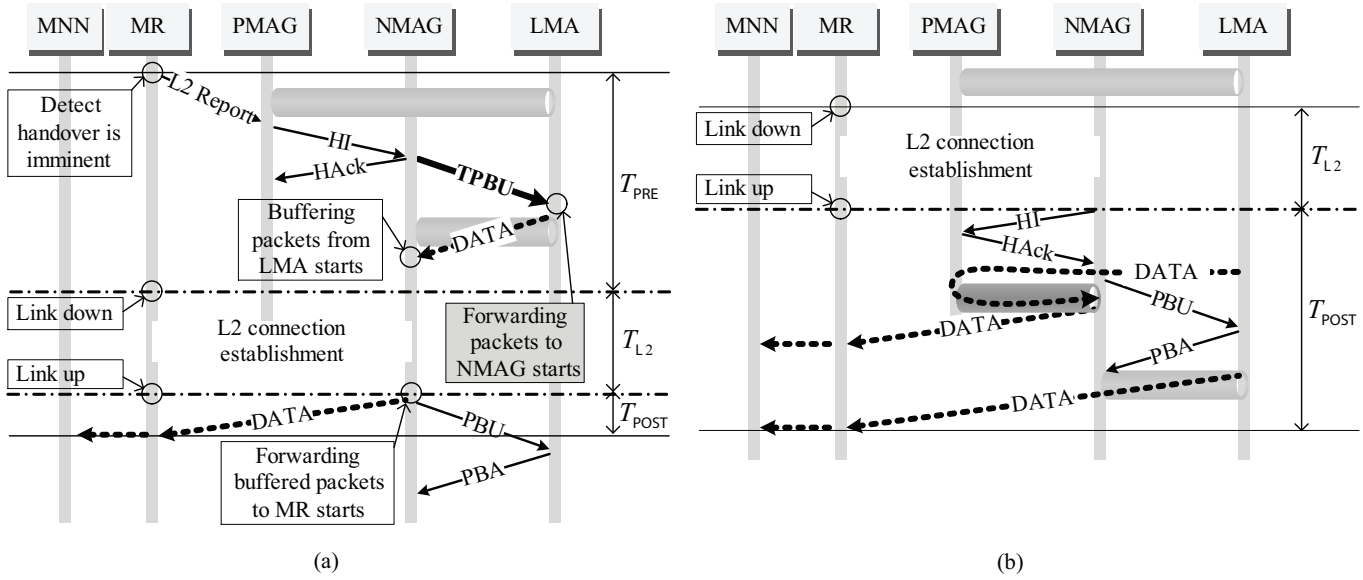

Fig. 3. Handover operation of IFP-NEMO: (a) The predictive mode and (b) the reactive mode.

ation in the predictive mode of the IFP-NEMO is defined in Fig. 3(a). The predictive mode of the IFP-NEMO is initiated with the MR's layer 2 handover report. The PMAG further transmits the HI message to the NMAG. The HI message includes the MR ID, HNP, and address of the LMA. On receiving the HI message, the NMAG creates a TPBU message using the received information. The TPBU message is the same as the PBU message, except that the binding lifetime is short. Further, the NMAG transmits the TPBU message to the LMA and the HAck message to the PMAG. When the LMA receives the TPBU message, it tentatively generates an additional entry in the BCE. The previous binding information for the MR is preserved in the BCE during handover because it is used to prevent ping-pong movements. For example, when the MR moves back to the PMAG during handover, the tentative binding expires, and the packets destined for the MNNs are transmitted back to the PMAG using the previous binding information in the BCE. As soon as the new binding is generated in the BCE of the LMA, the packets destined for the MNNs are directly forwarded to the NMAG. The NMAG receives and buffers the packets from the LMA during handover. When the PMAG receives the HAck message, a tunnel between the PMAG and the NMAG is established. However, the tunnel between the MAGs is not used during handover because the packets destined for the MNNs are directly forwarded to the NMAG. In the IFP-NEMO, the tunnel is retained for further use when the LMA cannot process the TPBU message or when the TPBU message cannot be delivered to the LMA. Upon completion of the layer 2 handover, the NMAG delivers the packets to the MR, thus completing the handover process. In addition, the NMAG transmits the PBU message to the LMA to confirm the movement of the MR. When the LMA receives the PBU message from the NMAG, it updates the BCE for the MR.

The reactive mode of the IFP-NEMO is illustrated in Fig. 3(b). We define the reactive mode of the IFP-NEMO by using the reactive mode of the FPMIPv6. Upon completion of the layer 2 handover, the NMAG transmits the HI message to the PMAG to establish a tunnel between the NMAG and the PMAG. Thus, before the registration process is completed, the packets destined for the MNNs are forwarded through this tunnel.

Table 1. Notations.

Notation	Description
$\alpha(K)$	Probability of K movements
ρ	Session to mobility ratio (SMR)
P_f	Probability of the predictive mode failure
t_w	Wireless link delay
t_l	Wired link delay
T_{L2}	Link switching delay
p_{wlf}	Probability of wireless link failure
$H_{\mathrm{LMA-MAG}}$	The number of hops between LMA and MAG
H_{MAGs}	The number of hops between MAGs
L_{PBU}	Length of the PBU message
L_{PBA}	Length of the PBA message
L_{TPBU}	Length of the TPBU message
L_{HI}	Length of the HI message
L_{HAck}	Length of the HAck message
L_{HD}	Length of a tunnel header
N_{MNN}	The number of MNNs
λ_p	Packet arrival rate
τ	Weight factor for tunneling
η	Weight factor for packet loss

IV. PERFORMANCE ANALYSIS

Here, we develop an analytical framework to investigate the handover performance of the IFP-NEMO as compared with that of the FP-NEMO, as in [4] and [25]–[27]. The analytical framework consists of mobility modeling, handover latency analysis, and cost analysis. We analyze the handover latencies and the

overall costs of the IFP-NEMO and FP-NEMO to evaluate the performances of these schemes. The notations used in the performance analysis are listed in Table 1.

A. Mobility Modeling

This section describes the mobility model and the probability of the predictive mode failure, P_f. The mobility model determines the movement rate of the MR, while P_f is used to combine the predictive mode and the reactive mode of the IFP-NEMO and FP-NEMO.

We derive probability $\alpha(K)$ that an MR moves across K RAs between two sessions. We assume that the intersession arrival time follows an exponential distribution with rate λ_S. The residence time of an MR in the MAG follows a general distribution with $1/\mu_L$, and its probability density function is $f_L(t)$. $f_L^*(s)$ denotes the Laplace transform of $f_s(t)$ and is obtained as

$$f_L^*(s) = \int_{t=0}^{\infty} e^{-st} f_L(t) dt. \tag{1}$$

Further, the Laplace-Stieltjes transform for an exponentially distributed random variable is obtained as follows [4]

$$f_L^*(s) = \int_{t=0}^{\infty} e^{-st} \mu_L e^{-\mu_L t} dt. \tag{2}$$

Let N_L be the number of subnet crossings during the intersession arrival time. Further, $Pr(N_L = K) = \alpha(K)$ is derived as follows [28]

$$\alpha(K) = \begin{cases} 1 - \frac{1 - f_L{}^*(\lambda_S)}{\rho}, & K = 0 \\ \frac{1}{\rho}[1 - f_L^*(\lambda_S)]^2 [f_L^*(\lambda_S)]^{K-1}, & K > 0 \end{cases} \tag{3}$$

where ρ is the SMR and $\rho = \lambda_S/\mu_L$ [4], [28].

In both FP-NEMO and IFP-NEMO, the additional signaling messages are exchanged between a PMAG and an NMAG, while the MR resides in the overlapping area between the PMAG and the NMAG. The predictive mode fails when the MR leaves the overlapping area before the transmission of the additional signaling messages is completed. When the predictive mode fails, the reactive mode is activated. Further, the probability of the predictive mode failure, P_f, must be obtained to evaluate the performances of the FP-NEMO and IFP-fNEMO. Fig. 4 shows the overlapping area of the boundary cells. Let T be a random variable for denoting the residence time in the overlapping area, that is, pending a layer 2 handover. P_f is obtained as follows [29]

$$P_f = \Pr(T < T_{\mathrm{PRE}}) = \int_0^{T_{\mathrm{PRE}}} f_T(t) dt,\ T \geq 0 \tag{4}$$

where T_{PRE} is the required time for additional signaling in FP-NEMO or IFP-NEMO before the layer 2 handover. If we assume that T is exponentially distributed [30], $f_T(t) = \lambda e^{-\lambda t}$. Therefore, P_f is obtained as

$$P_f = 1 - e^{-\lambda T_{\mathrm{PRE}}} \tag{5}$$

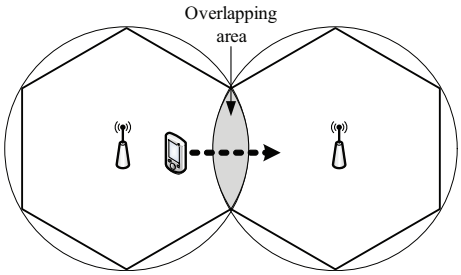

Fig. 4. Overlapping area between boundary cells.

where λ is the arrival rate of the MR in the overlapping area. Using the movement rate, $\sum_{i=0}^{\infty} i\alpha(i)$, we can derive λ as follows

$$\begin{aligned} \lambda &= \theta \sum_{i=0}^{\infty} i\alpha(i) \\ &= \theta \sum_{i=0}^{\infty} \frac{i}{\rho} [1 - f_L^*(\lambda_s)]^2 [f_L^*(\lambda_s)]^{i-1} \end{aligned} \tag{6}$$

where θ is the weight factor, which is defined by the network environment, such as the radius of a cell and the overlapping area.

B. Analysis of Handover Latency

We define the handover latency as the time interval between the moment of detection of the impending handover and the moment the MR directly receives the first packets from the LMA in the new network. The handover latencies of the FP-NEMO and IFP-NEMO can be obtained as shown in Figs. 2 and 3, respectively. In both FP-NEMO and IFP-NEMO, the handover latencies are divided into those in the predictive mode and those in the reactive mode, respectively. Further, the handover latencies of FP-NEMO, $T_{\mathrm{HO}}^{(\mathrm{FPN})}$, and IFP-fNEMO, $T_{\mathrm{HO}}^{(\mathrm{IFPN})}$, are obtained as follows

$$T_{\mathrm{HO}}^{(\mathrm{FPN})} = (1 - P_f) T_{\mathrm{HO}}^{(p\mathrm{FPN})} + P_f T_{\mathrm{HO}}^{(r\mathrm{FPN})} \tag{7}$$

$$T_{\mathrm{HO}}^{(\mathrm{IFPN})} = (1 - P_f) T_{\mathrm{HO}}^{(p\mathrm{IFPN})} + P_f T_{\mathrm{HO}}^{(r\mathrm{IFPN})} \tag{8}$$

where $T_{\mathrm{HO}}^{(p\mathrm{FPN})}$, $T_{\mathrm{HO}}^{(r\mathrm{FPN})}$, $T_{\mathrm{HO}}^{(p\mathrm{IFPN})}$, and $T_{\mathrm{HO}}^{(r\mathrm{IFPN})}$ are the handover latencies in the predictive mode and reactive mode of the FP-NEMO and IFP-NEMO, respectively. With reference to Fig. 2, $T_{\mathrm{HO}}^{(p\mathrm{FPN})}$ and $T_{\mathrm{HO}}^{(r\mathrm{FPN})}$ are expressed as follows

$$\begin{aligned} T_{\mathrm{HO}}^{(p\mathrm{FPN})} &= T_{\mathrm{PRE}}^{(p\mathrm{FPN})} + T_{\mathrm{L2}} + T_{\mathrm{POST}}^{(p\mathrm{FPN})} \\ &= 2t_w + 2\left(H_{\mathrm{MAGs}} + H_{\mathrm{LMA-MAG}}\right) t_l + T_{\mathrm{L2}} \end{aligned} \tag{9}$$

$$\begin{aligned} T_{\mathrm{HO}}^{(r\mathrm{FPN})} &= T_{\mathrm{L2}} + T_{\mathrm{POST}}^{(r\mathrm{FPN})} \\ &= 2t_w + 2H_{\mathrm{LMA-MAG}} t_l + T_{\mathrm{L2}} \end{aligned} \tag{10}$$

where T_{L2} is the link switching delay. $T_{\mathrm{PRE}}^{(p\mathrm{FPN})}$, $T_{\mathrm{POST}}^{(p\mathrm{FPN})}$, and $T_{\mathrm{POST}}^{(r\mathrm{FPN})}$ are the partial delays in the FP-NEMO. For the calculation of the delays consisting of the handover latency, the wired link delay, t_w, and the wireless link delay, t_l, are defined. H_{MAGs} and $H_{\mathrm{LMA-MAG}}$ are the hop distances between the MAGs and between the LMA and the MAG, respectively.

In the FP-NEMO, $T_{\mathrm{HO}}^{(p\mathrm{IFPN})}$ and $T_{\mathrm{HO}}^{(r\mathrm{IFPN})}$ are calculated, referring to Fig. 3, as follows

$$\begin{aligned} T_{\mathrm{HO}}^{(p\mathrm{IFPN})} &= T_{\mathrm{PRE}}^{(p\mathrm{IFPN})} + T_{\mathrm{L2}} + T_{\mathrm{POST}}^{(p\mathrm{IFPN})} \\ &= 2t_w + \left\{ H_{\mathrm{MAGs}} \right. \\ &\quad \left. + \max\left(H_{\mathrm{MAGs}}, H_{\mathrm{LMA-MAG}}\right) t_l \right\} + T_{\mathrm{L2}} \qquad (11) \\ T_{\mathrm{HO}}^{(r\mathrm{IFPN})} &= T_{\mathrm{L2}} + T_{\mathrm{POST}}^{(r\mathrm{IFPN})} \\ &= t_w + 2\left(H_{\mathrm{MAGs}} + H_{\mathrm{LMA-MAG}}\right) t_l + T_{\mathrm{L2}} \qquad (12) \end{aligned}$$

where $T_{\mathrm{PRE}}^{(p\mathrm{IFPN})}$, $T_{\mathrm{POST}}^{(p\mathrm{IFPN})}$, and $T_{\mathrm{POST}}^{(r\mathrm{IFPN})}$ are the partial delays in the IFP-NEMO. When the MAG is too far from the LMA, $T_{\mathrm{HO}}^{(p\mathrm{IFPN})}$ is the same as $T_{\mathrm{HO}}^{(p\mathrm{FPN})}$. This is because the TPBU message cannot arrive at the LMA during handover. For instance, if $H_{\mathrm{LMA-MAG}} t_l > T_{\mathrm{L2}}$, then $T_{\mathrm{HO}}^{(p\mathrm{IFPN})} = T_{\mathrm{HO}}^{(p\mathrm{FPN})}$.

t_l and t_w are obtained by summing the transmission delay, propagation delay, and processing delay. t_l is expressed as follows

$$t_l = \frac{L}{B_{wd}} + T_{wd} + \varpi_q \qquad (13)$$

where L is the length of a packet, B_{wd} is the bandwidth of the wired link, T_{wd} is the propagation delay on the wired link, and ϖ_q is the average queueing delay at each router in the Internet. In the case of the wireless link delay, the wireless link failure is considered. Let n_f and P_{nf} be the number of wireless link failures and the probability that a message transmission over the wireless link fails n_f times before the message is successfully transmitted, respectively [4], [31]. The mean number of n_f, $E[n_f]$, is expressed as follows [31]

$$E[n_f] = \sum_{n_f=0}^{\infty} n_f P_{n_f} = \frac{p_{wlf}}{1 - p_{wlf}} \qquad (14)$$

where p_{wlf} is the probability of the wireless link failure. Thus, the wireless link delay, t_w, is calculated as follows

$$\begin{aligned} t_w &= \left(\frac{L}{B_{wl}} + T_{wl} + T_p\right) \\ &\quad + E[n_f]\left(\frac{L}{B_{wl}} + T_{wl} + T_p + T_{\mathrm{wait}}\right) \qquad (15) \end{aligned}$$

where T_{wait} is the waiting time to determine the loss of a message, B_{wl} is the bandwidth of the wireless link, T_{wl} is the propagation delay on the wireless link, and T_p is the processing time. Let $T_{\mathrm{wait}} = \gamma(\frac{L}{B_{wl}} + T_{wl} + T_p)$ because the waiting time can be determined by the round trip time, where γ is the weight factor for the waiting time. Further, (15) becomes

$$t_w = \left(\frac{1 + \gamma p_{wlf}}{1 - p_{wlf}}\right)\left(\frac{L}{B_{wl}} + T_{wl} + T_p\right). \qquad (16)$$

C. Cost Analysis

Here, we derive the cost functions of the signaling overhead and the packet tunneling to investigate the performances of the FP-NEMO and IFP-NEMO. The signaling overhead is defined as the handover signaling cost incurred during a session and is calculated by the product of the message length and the number of hops [12]. The packet tunneling cost is defined as the additional tunneling overhead incurred during handover. Therefore, the overall costs of the FP-NEMO, $C^{(\mathrm{FP-NEMO})}$, and the IFP-NEMO, $C^{(\mathrm{IFP-NEMO})}$, are expressed, respectively as follows

$$C^{(\mathrm{FP-NEMO})} = C_{\mathrm{SG}}^{(\mathrm{FPN})} + C_{\mathrm{PT}}^{(\mathrm{FPN})} \qquad (17)$$

$$C^{(\mathrm{IFP-NEMO})} = C_{\mathrm{SG}}^{(\mathrm{IFPN})} + C_{\mathrm{PT}}^{(\mathrm{IFPN})} \qquad (18)$$

where $C_{\mathrm{SG}}^{(\mathrm{FPN})}$, $C_{\mathrm{PT}}^{(\mathrm{FPN})}$, $C_{\mathrm{SG}}^{(\mathrm{IFPN})}$, and $C_{\mathrm{PT}}^{(\mathrm{IFPN})}$ are the signaling overheads and the packet tunneling costs of FP-NEMO and IFP-NEMO, respectively. $C_{\mathrm{SG}}^{(\mathrm{FPN})}$ and $C_{\mathrm{SG}}^{(\mathrm{IFPN})}$ are divided into the predictive mode and the reactive mode, respectively and are obtained as follows

$$C_{\mathrm{SG}}^{(\mathrm{FPN})} = (1 - P_f) C_{\mathrm{SG}}^{(p\mathrm{FPN})} + P_f C_{\mathrm{SG}}^{(r\mathrm{FPN})} \qquad (19)$$

$$C_{\mathrm{SG}}^{(\mathrm{IFPN})} = (1 - P_f) C_{\mathrm{SG}}^{(p\mathrm{IFPN})} + P_f C_{\mathrm{SG}}^{(r\mathrm{IFPN})} \qquad (20)$$

where $C_{\mathrm{SG}}^{(p\mathrm{FPN})}$, $C_{\mathrm{SG}}^{(r\mathrm{FPN})}$, $C_{\mathrm{SG}}^{(p\mathrm{IFPN})}$, and $C_{\mathrm{SG}}^{(r\mathrm{IFPN})}$ are the signaling costs in the predictive mode and reactive mode of the FP-NEMO and IFP-NEMO, respectively. These parameters are obtained, referring to Figs. 2 and 3 as follows

$$C_{\mathrm{SG}}^{(p\mathrm{FPN})} = \sum_{i=0}^{\infty} i\alpha(i)\left(S_{\mathrm{MAGs}} + S_{\mathrm{LMA-MAG}}^{c1}\right) \qquad (21)$$

$$C_{\mathrm{SG}}^{(p\mathrm{IFPN})} = \sum_{i=0}^{\infty} i\alpha(i)\left(S_{\mathrm{MAGs}} + S_{\mathrm{LMA-MAG}}^{c2}\right) \qquad (22)$$

$$C_{\mathrm{SG}}^{(r\mathrm{FPN})} = \sum_{i=0}^{\infty} i\alpha(i) S_{\mathrm{LMA-MAG}}^{c1} \qquad (23)$$

$$C_{\mathrm{SG}}^{(r\mathrm{IFPN})} = \sum_{i=0}^{\infty} i\alpha(i)\left(S_{\mathrm{MAGs}} + S_{\mathrm{LMA-MAG}}^{c1}\right) \qquad (24)$$

where S_{MAGs} is the sum of the signaling costs incurred between the MAGs, and $S_{\mathrm{LMA-MAG}}^{c1}$ and $S_{\mathrm{LMA-MAG}}^{c2}$ are the sums of the signaling costs incurred between the LMA and the MAG. $S_{\mathrm{MAGs}} = H_{\mathrm{MAGs}}(L_{\mathrm{HI}} + L_{\mathrm{HAck}})$, $S_{\mathrm{LMA-MAG}}^{c1} = H_{\mathrm{LMA-MAG}}(L_{\mathrm{PBU}} + L_{\mathrm{PBA}})$, and $S_{\mathrm{LMA-MAG}}^{c2} = H_{\mathrm{LMA-MAG}}(L_{\mathrm{TPBU}} + L_{\mathrm{PBU}} + L_{\mathrm{PBA}})$. $\sum_{i=0}^{\infty} i\alpha(i)$ denotes the handover rate.

The packet tunneling costs of FP-NEMO and IFP-NEMO are obtained as follows

$$C_{\mathrm{PT}}^{(\mathrm{FPN})} = (1 - P_f) C_{\mathrm{PT}}^{(p\mathrm{FPN})} + P_f C_{\mathrm{PT}}^{(r\mathrm{FPN})} \qquad (25)$$

$$C_{\mathrm{PT}}^{(\mathrm{IFPN})} = (1 - P_f) C_{\mathrm{PT}}^{(p\mathrm{IFPN})} + P_f C_{\mathrm{PT}}^{(r\mathrm{IFPN})} \qquad (26)$$

where $C_{\mathrm{PT}}^{(p\mathrm{FPN})}$, $C_{\mathrm{PT}}^{(r\mathrm{FPN})}$, $C_{\mathrm{PT}}^{(p\mathrm{IFPN})}$, and $C_{\mathrm{PT}}^{(r\mathrm{IFPN})}$ are the packet tunneling costs in the predictive mode and reactive mode of the FP-NEMO and IFP-NEMO, respectively.

In the predictive mode of the FP-NEMO, the packets destined for the MNNs are tunneled between the MAGs after a tunnel is established, while in the reactive mode, they are lost during handover. With reference to Fig. 2, the packet tunneling costs of the FP-NEMO are obtained as follows

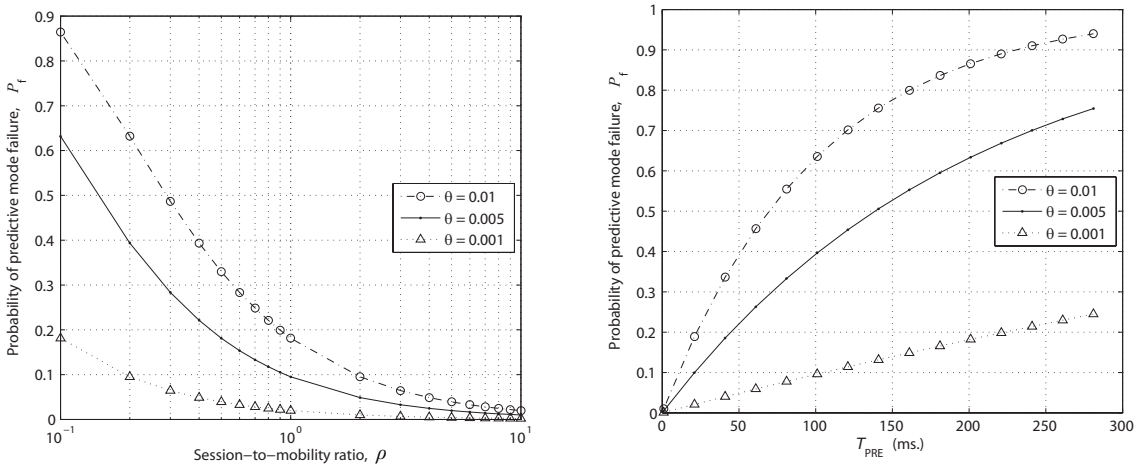

Fig. 5. Probability of predictive mode failure as a function of ρ, θ, and T_{PRE}: (a) P_f vs. ρ and θ and (b) P_f vs. T_{PRE} and θ.

$$C_{\mathrm{PT}}^{(p\mathrm{FPN})} = \sum_{i=0}^{\infty} i\alpha(i)\Bigg\{ N_{\mathrm{MNN}}\lambda_p\Bigg(P_{\mathrm{LMA-MAG}} T_{\mathrm{HO}}^{(p\mathrm{FPN})} + \tau P_{\mathrm{MAGs}} T_{\mathrm{TNL}}^{(\mathrm{pFPN})}\Bigg)\Bigg\} \tag{27}$$

$$C_{\mathrm{PT}}^{(r\mathrm{FPN})} = \sum_{i=0}^{\infty} i\alpha(i)\Bigg[N_{\mathrm{MNN}}\lambda_p\Bigg\{ \eta P_{\mathrm{LMA-MAG}} T_{\mathrm{LOSS}}^{(r\mathrm{FPN})} + P_{\mathrm{LMA-MAG}}\left(T_{\mathrm{HO}}^{(r\mathrm{FPN})} - T_{\mathrm{LOSS}}^{(r\mathrm{FPN})}\right)\Bigg\}\Bigg] \tag{28}$$

where N_{MNN} and λ_p are the number of MNNs attached to the MR and the packet arrival rate, respectively. η is the weight factor for the packet loss, which denotes the number of retransmissions owing to packet loss. P_{MAGs} and $P_{\mathrm{LMA-MAG}}$ are the unit costs of the packet tunnel overheads between the MAGs and between the LMA and the MAG, respectively, and are expressed as $P_{\mathrm{MAGs}} = H_{\mathrm{MAGs}}(L_{\mathrm{HD}} + L_{\mathrm{HD}})$ and $P_{\mathrm{LMA-MAG}} = H_{\mathrm{LMA-MAG}} L_{\mathrm{HD}}$. $T_{\mathrm{TNL}}^{(p\mathrm{FPN})}$ and $T_{\mathrm{LOSS}}^{(r\mathrm{FPN})}$ are the delays during the tunneling in the predictive mode and during the packet loss in the reactive mode, respectively. $T_{\mathrm{TNL}}^{(p\mathrm{FPN})} = T_{\mathrm{L2}} + 2H_{\mathrm{LMA-MAG}} t_l$ and $T_{\mathrm{LOSS}}^{(r\mathrm{FPN})} = T_{\mathrm{L2}} + t_w + H_{\mathrm{LMA-MAG}} t_l$.

In the predictive mode of the IFP-NEMO, the packets destined for the MR are directly forwarded to the PMAG or NMAG, regardless of handover. However, when the MR is too far from the LMA, the TPBU message does not arrive at the LMA during T_{PRE}. In this case, the packets destined for the MR are tunneled as in the FP-NEMO. Thus, the packet tunneling costs of the IFP-NEMO are expressed, as shown in Fig. 3, as follows

$$C_{\mathrm{PT}}^{(p\mathrm{IFPN})} = \sum_{i=0}^{\infty} i\alpha(i)\Bigg\{ N_{\mathrm{MNN}}\lambda_p\Bigg(P_{\mathrm{LMA-MAG}} T_{\mathrm{HO}}^{(p\mathrm{IFPN})} + \tau P_{\mathrm{MAGs}} T_{\mathrm{TNL}}^{(p\mathrm{IFPN})}\Bigg)\Bigg\} \tag{29}$$

$$C_{\mathrm{PT}}^{(r\mathrm{IFPN})} = \sum_{i=0}^{\infty} i\alpha(i)\Bigg[N_{\mathrm{MNN}}\lambda_p\Bigg\{ \eta P_{\mathrm{LMA-MAG}} T_{\mathrm{LOSS}}^{(r\mathrm{IFPN})} + \left(P_{\mathrm{LMA-MAG}} + \tau P_{\mathrm{MAGs}}\right) T_{\mathrm{TNL}}^{(r\mathrm{IFPN})} + P_{\mathrm{LMA-MAG}} \left(T_{\mathrm{HO}}^{(r\mathrm{IFPN})} - T_{\mathrm{LOSS}}^{(r\mathrm{IFPN})} - T_{\mathrm{TNL}}^{(r\mathrm{IFPN})}\right)\Bigg\}\Bigg] \tag{30}$$

where $T_{\mathrm{TNL}}^{(p\mathrm{IFPN})}$ is the delay during tunneling in the predictive mode. $T_{\mathrm{TNL}}^{(p\mathrm{IFPN})} = \min(\max(H_{\mathrm{LMA-MAG}} t_l - H_{\mathrm{MAGs}} t_l, 0), T_{\mathrm{TNL}}^{(p\mathrm{FPN})})$. $T_{\mathrm{LOSS}}^{(r\mathrm{IFPN})}$ and $T_{\mathrm{TNL}}^{(r\mathrm{IFPN})}$ are the delays during the packet loss and tunneling in the reactive mode, respectively. $T_{\mathrm{LOSS}}^{(r\mathrm{IFPN})} = T_{\mathrm{L2}} + H_{\mathrm{MAGs}} t_l$ and $T_{\mathrm{TNL}}^{(r\mathrm{IFPN})} = \left(H_{\mathrm{MAGs}} + H_{\mathrm{LMA-MAG}}\right) t_l$.

V. NUMERICAL RESULTS

In this section, we demonstrate the comparative numerical results of the FP-NEMO and IFP-NEMO in terms of the handover latency and overall cost. The parameters used in this analysis are defined as follows $L = 512$ Kbytes, $B_{wd} = 1$ Gbps, $B_{wl} = 54$ Mbps, $T_{wd} = 0.5$ ms, $T_{wl} = 2$ ms, $\varpi_q = 0.5$, $T_p = 0.5$ ms, $T_{L2} = 58.74$ ms, $N_{\mathrm{MNN}} = 5$, $\lambda_p = 50$ pakets/s, $\gamma = 1$, $\eta = 2$, $H_{\mathrm{LMA-MAG}} = 5$, $H_{\mathrm{MAGs}} = 1$, $L_{\mathrm{PBU}} = L_{\mathrm{PBU}} = L_{\mathrm{TPBU}} = 76$ bytes, $L_{\mathrm{HI}} = S_{\mathrm{HAck}} = 52$ bytes, and $L_{\mathrm{HD}} = 40$ bytes [4], [12], [31]–[33].

A. Probability of Predictive Mode Failure

The probability of predictive mode failure, P_f, can be obtained by the MR movement rate and the network environment. When P_f is low, the FP-NEMO and IFP-NEMO more frequently operate in the predictive mode. Fig. 5(a) shows P_f as a function of ρ and θ. When ρ is high, the session rate is higher than the handover rate and the mobility is low. On the other hand, the session rate is lower than the handover rate, when ρ is low. In other words, ρ denotes the MR velocity. Thus, P_f becomes high when the MR velocity is high. θ denotes the net-

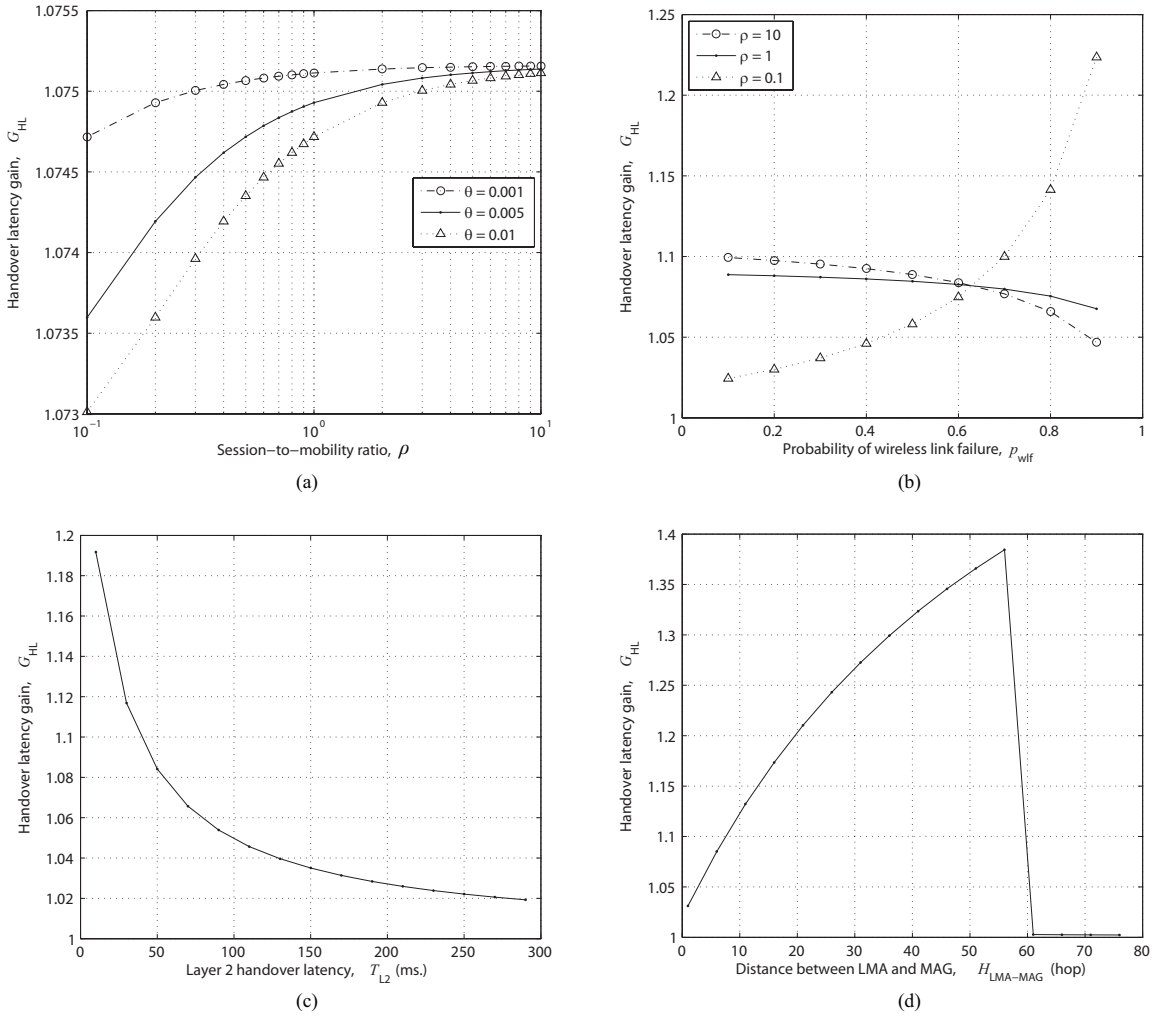

Fig. 6. Relative handover latency gains as functions of ρ, θ, p_{wlf}, T_{L2}, and $H_{\mathrm{LMA-MAG}}$: (a) G_{HL} vs. ρ and θ, (b) G_{HL} vs. p_{wlf} and ρ, (c) G_{HL} vs. T_{L2}, and G_{HL} vs. $H_{\mathrm{LMA-MAG}}$.

work environment. For example, when θ is low, it indicates that the radius of a cell or the overlapping area is large. P_f becomes low when θ is low.

As shown in Fig. 5(b), the changes in P_f are depicted by T_{PRE}. T_{PRE} is the time required for the additional signaling in FP-NEMO or IFP-NEMO before the layer 2 handover. Hence, P_f becomes low when T_{PRE} is short. T_{PRE} is dependent on the transmission delays between an MR, an MAG, and MAGs, and therefore, it gradually decreases overtime. In addition, P_f becomes low.

B. Relative Handover Latency Gain

In this section, we compare the IFP-NEMO with the FP-NEMO in terms of the handover latency. For this, we define the relative handover latency gain as follows

$$G_{\mathrm{HL}} = \frac{T_{\mathrm{HO}}^{(\mathrm{FPN})}}{T_{\mathrm{HO}}^{(\mathrm{IFPN})}}. \tag{31}$$

When $G_{\mathrm{HL}} > 1$, the IFP-NEMO outperforms the FP-NEMO.

Fig. 6(a) shows the relative handover latency gains as functions of ρ and θ. As ρ increases, the relative handover latency gains increase. When ρ is high, the mobility is low and the session arrival rate is high. Thus, the handover performance of the IFP-NEMO is better than that of the FP-NEMO, where the vehicles move at a low velocity as in urban areas. In addition, the relative handover latency gain increases when θ is low. This implies that the handover performance of the IFP-NEMO is better than that of the FP-NEMO, where the radius of a cell or the overlapping area is large. In addition, even when ρ is low and θ is high, the IFP-NEMO outperforms the FP-NEMO.

As shown in Fig. 6(b), the relative handover latency gains as functions of p_{wlf} and ρ are depicted. The probability of the wireless link failure, p_{wlf}, denotes the status of the wireless link. For example, when p_{wlf} is low, the wireless link is in good condition without link errors. The handover performance of the IFP-NEMO is better than that of the FP-NEMO when p_{wlf} is low and ρ is high. On the other hand, when p_{wlf} is high and ρ is low, the handover performance of the IFP-NEMO is better than that of the FP-NEMO. In other words, the IFP-NEMO outperforms the FP-NEMO even when the error rate of the wireless link is high and the vehicles move fast.

The relative handover latency gain as a function of T_{L2} is il-

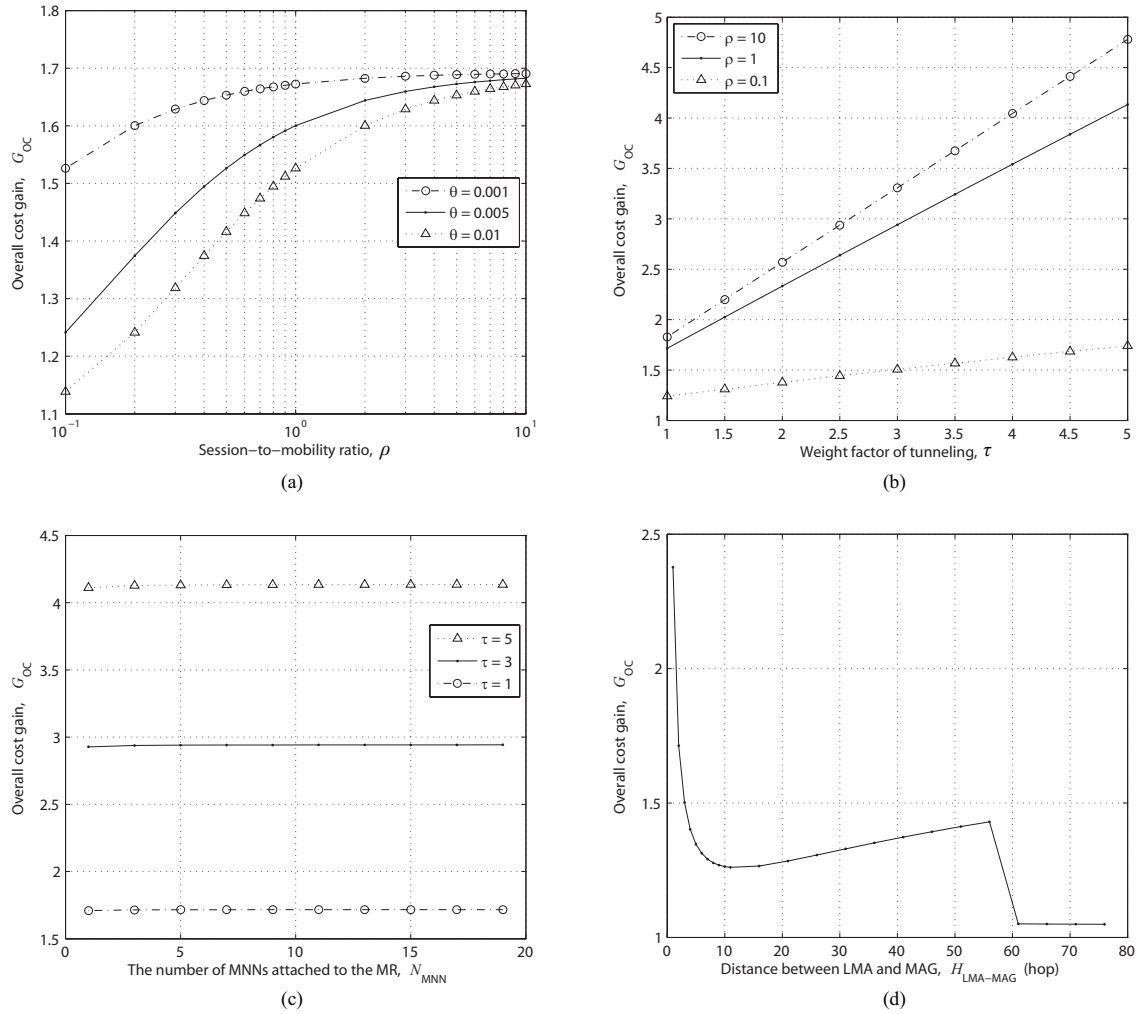

Fig. 7. Relative overall cost gains as functions of ρ, θ, τ, N_{MNN}, and $H_{\mathrm{LMA-MAG}}$: (a) G_{OC} vs. ρ and θ, (b) G_{OC} vs. τ and ρ, (c) G_{OC} vs. N_{MNN} and τ, and G_{OC} vs. $H_{\mathrm{LMA-MAG}}$.

lustrated in Fig. 6(c). T_{L2}, which is the link switching delay, depends on the wireless technology. As T_{L2} decreases, the relative handover latency gains increase. T_{L2} can become shorter as the wireless technology is improved. Therefore, the IFP-NEMO can highly improve the handover performance, because more advanced technologies will emerge in the future.

Fig. 6(d) illustrates the relative handover latency gain as a function of $H_{\mathrm{LMA-MAG}}$, which is the distance between the LMA and the MAG. The handover latency of the FP-NEMO is higher than that of the IFP-NEMO as $H_{\mathrm{LMA-MAG}}$ increases. However, when $H_{\mathrm{LMA-MAG}} > 60$, the handover latency of the IFP-NEMO is the same as that of the FP-NEMO. This is because the TPBU procedure cannot be completed during handover. Nevertheless, the IFP-NEMO generally outperforms the FP-NEMO, because the MAG is not too far from the LMA.

C. Relative Overall Cost Gain

For the evaluation of the IFP-NEMO performance as compared with that of the FP-NEMO, we define the relative overall cost gain as follows

$$G_{\mathrm{OC}} = \frac{C^{(\mathrm{FP-NEMO})}}{C^{(\mathrm{IFP-NEMO})}}. \tag{32}$$

When $G_{\mathrm{OC}} > 1$, the IFP-NEMO outperforms the FP-NEMO.

The relative overall cost gains depending on ρ and θ are illustrated in Fig. 7(a). As ρ increases, the relative overall cost gains increase. As shown in Fig. 6(a), the handover performance of the IFP-NEMO is better than that of the FP-NEMO, where the vehicles move at a low velocity. In addition, the relative overall cost gain increases when θ is low. Therefore, the IFP-NEMO considerably outperforms the FP-NEMO, where the radius of a cell or the overlapping area is large and the movement rate is low as in urban areas.

The relative overall cost gains depending on τ and ρ are plotted, as shown in Fig. 7(b). τ denotes the degree of traffic density in the link between the PMAG and the NMAG. When the traffic on that link increases, τ increases. In general, the relative overall cost gains increase as τ increases, because the IFP-NEMO does not use the tunnel between the PMAG and the NMAG. Even when τ is low, the IFP-NEMO outperforms the FP-NEMO. This

is because the handover latency of the IFP-NEMO is lower than that of the FP-NEMO. The relative overall cost gains increase as ρ increases because the packet tunneling cost is highly affected by high ρ. Additionally, the handover performance of the IFP-NEMO is not lower than that of the FP-NEMO, even when ρ is low.

Fig. 7(c) shows the relative overall cost gains depending on N_{MNN} and τ. N_{MNN} is the number of MNNs attached to an MR. The IFP-NEMO improves the handover performance of the FP-NEMO, regardless of N_{MNN}. Thus, the IFP-NEMO is more efficient than the FP-NEMO, where many users simultaneously use the Internet services in the case of public transportation, such as in buses and trains. In particular, when τ is high, the IFP-NEMO considerably outperforms the FP-NEMO.

As shown in Fig. 7(d), the relative overall cost gain is depicted depending on $H_{\mathrm{LMA-MAG}}$. When $H_{\mathrm{LMA-MAG}}$ is short, the handover performance of the IFP-NEMO becomes high as $H_{\mathrm{LMA-MAG}}$ decreases. This is because the duration of tunneling between the PMAG and the NMAG becomes significantly long in the IFP-NEMO. On the other hand, when $H_{\mathrm{LMA-MAG}} > 10$, the handover latency of the FP-NEMO is higher than that of the IFP-NEMO, and therefore, the handover performance of the IFP-NEMO becomes high as $H_{\mathrm{LMA-MAG}}$ increases. When $H_{\mathrm{LMA-MAG}} > 60$, the handover performance of the IFP-NEMO becomes low. The reason is the same as that depicted in Fig. 6(d). As a result, because the MAG is not too far from the LMA, the IFP-NEMO generally outperforms the FP-NEMO.

VI. CONCLUSIONS

FP-NEMO emerged to accelerate handover for the P-NEMO by anticipating an impending handover. Even though FP-NEMO enhances the handover performance, it can incur a tunneling burden between the PMAG and the NMAG during handover. In this study, we highlight the problem of the tunneling burden, which was not properly investigated in the previous studies. Thus, we propose an IFP-NEMO to eliminate the tunneling burden by registering a new CoA in advance.

For the evaluation of the IFP-NEMO performance as compared with that of the FP-NEMO, we have developed an analytical framework. In the analytical framework, we have taken into account two modes of fast handover schemes. The numerical results demonstrate the handover performance of the IFP-NEMO in terms of the handover latency and overall cost. In general, the IFP-NEMO improves the handover performance of the FP-NEMO. In particular, the IFP-NEMO considerably outperforms the FP-NEMO, where the radius of a cell or the overlapping area is large and the movement rate is low as in urban areas.

REFERENCES

[1] S. Cespedes and X. Shen, "IP mobility management for vehicular communication networks: Challenges and solutions," *IEEE Commun. Mag.*, vol. 49, no. 5, pp. 187–194, May 2011.

[2] V. Devarapalli, R. Wakikawa, A. Petrescu, and P. Thubert, "Network mobility (NEMO) basic support protocol," *RFC* 3963, Jan. 2005.

[3] T. Ernst, "The information technology era of the vehicular industry," *ACM SIGCOMM Comput. Commun. Rev.*, vol. 36, no. 2, pp. 49–52, Apr. 2006.

[4] J.-H. Lee, T. Ernst, and N. Chilamkurti, "Performance analysis of PMIPv6 based network mobility for intelligent transportation systems," *IEEE Trans. Veh. Technol.*, vol. 61, pp. 74–85, Jan. 2012.

[5] ISO Draft DIS 21210, "Intelligent transport systems – communications access for land mobiles (CALM) – IPv6 networking," Feb. 2009.

[6] ETSI TS 102 636-3, "Intelligent transport systems (ITS); Vehicular communications; GeoNetworking; Part 3: Network architecture," v1.1.1, Mar. 2010.

[7] ETSI TS 102 636-4-1, "Intelligent transport systems (ITS); Vehicular communications; Part 4: Geographical addressing and forwarding for point-to-point and point-to-multipoint communications; Sub-part 1: Media-independent functionality," v0.0.9, Nov. 2010.

[8] C. Perkins, D. Johnson, and J. Arkko, "Mobility support in IPv6," *RFC* 6275, July 2011.

[9] M. Calderon, C. J. Bernardos, M. Bagnulo, I. Soto, and A. de la Oliva, "Design and experimental evaluation of a route optimization solution for NEMO," *IEEE J. Sel. Areas Commun.*, vol. 24, no. 9, pp. 1702–1716, Sept. 2006.

[10] H. Petander, E. Perera, K.-C. Lan, and A. Seneviratne, "Measuring and improving the performance of network mobility management in IPv6 networks," *IEEE J. Sel. Areas Commun.*, vol. 24, no. 9, pp. 1671–1681, Sept. 2006.

[11] I. C. Chang and C. H. Chou, "HCoP-B: A hierarchical care-of prefix with BUT scheme for nested mobile networks," *IEEE Trans. Veh. Technol.*, vol. 58, pp. 2942–2965, July 2009.

[12] S. Pack, T. Kwon, Y. Choi, and E. Paik, "An adaptive network mobility support protocol in hierarchical mobile IPv6 networks," *IEEE Trans. Veh. Technol.*, vol. 58, pp. 3627–3639, Sept. 2009.

[13] C. M. Huang, C. H. Lee, and J. R. Zheng, "A novel SIP-based route optimization for network mobility," *IEEE J. Sel. Areas Commun.*, vol. 24, no. 9, pp. 1682–1690, Sept. 2009.

[14] H. J. Lim, M. Kim, J.-H. Lee, and T. M. Chung, "Route optimization in nested NEMO: Classification, evaluation, and analysis from NEMO fringe stub perspective," *IEEE Trans. Mob. Comput.*, vol. 8, pp. 1554–1572, Nov. 2009.

[15] A. Z. M. Shahriar, M. Atiquzzaman, and W. Ivancic, "Route optimization in network mobility: Solutions, classification, comparison, and future research directions," *IEEE Commun. Surveys Tutorials*, vol. 12, no. 1, pp. 24–38, 1st Quarter 2010.

[16] R. Kong, J. Feng, R. Gao, and H. Zhou, "A new route optimization scheme for network mobility: Combining ORC protocol with RRH and using quota mechanism," *J. Commun. Netw.*, vol. 14, no. 1, pp. 91–103, Feb. 2012.

[17] S. Gundavelli, K. Leung, V. Devarapalli, K. Chowdhury, and B. Patil, "Proxy mobile IPv6," *RFC* 5213, Aug. 2008.

[18] I. Soto, C. J. Bernardos, M. Calderon, A. Banchs, and A. Azcorra, "NEMO-enabled localized mobility support for Internet access in automotive scenarios," *IEEE Commun. Mag.*, vol. 47, no. 5, pp. 152–159, May 2009.

[19] Z. Yan, H. Zhou, and I. You, "N-NEMO: A comprehensive network mobility solution in proxy mobile IPv6 network," *J. WUA*, vol. 1, no. 2/3, pp. 52–70, Sept. 2010.

[20] J.-H. Lee and T. Ernst, "Lightweight network mobility within PMIPv6 for transportation systems," *IEEE Syst. J.*, vol. 5, no. 3, pp. 352–361, Sept. 2011.

[21] S. Ryu and Y. Mun, "The tentative and early binding update for mobile IPv6 fast handover," in *Proc. MSN 2005*, *LNCS*, vol. 3794, Dec. 2005, pp.825–835.

[22] S. Ryu and Y. Mun, "A scheme to enhance TEBU scheme of fast handovers for mobile IPv6," in *Int. Conf. Embedded Software Systems*, *LNCS*, vol. 4523, May 2007, pp. 773–782.

[23] S. Ryu, J.-W. Choi, and K.-J. Park, "A scheme improving fast PMIPv6-based network mobility by eliminating tunneling overload for ITS," in *Proc. IV*, June 2012.

[24] H. Yokota, K. Chowdhury, R. Koodli, B. Patil, and F. Xia, "Fast handovers for proxy mobile IPv6," *RFC* 5949, Sept. 2010.

[25] J. Xie and I. Akyildiz, "A distributed dynamic regional location management scheme for mobile IP," *IEEE Trans. Mob. Comput.*, vol. 1, no. 3, pp. 163–175, July/Sept. 2002.

[26] Y. Fang, "Movement-based mobility management and trade off analysis for wireless mobile networks," *IEEE Trans. Comput.*, vol. 52, no. 6, pp. 791–803, June 2003.

[27] C. Makaya and S. Pierre, "An analytical framework for performance evaluation of IPv6-based mobility management protocols," *IEEE Trans. Wireless Commun.*, vol. 7, pp. 972–983, Mar. 2008.

[28] Y.-B. Lin, "Reducing location update cost in a PCS network," *IEEE/ACM Trans. Netw.*, vol. 5, no. 1, pp. 25–33, Feb. 1997.

[29] S. Ryu, K. Lee, and Y. Mun, "Optimized fast handover scheme in mobile

IPv6 networks to support mobile users for cloud computing," *J. Supercomput.*, vol. 59, no. 2, pp. 658–675, Jan. 2012.
[30] Y.-B. Lin, "Modeling techniques for large-scale PCS networks," *IEEE Commun. Mag.*, vol. 35, no. 2, pp. 102–107, Feb. 1997.
[31] J. McNair, I. F. Akyildiz, and M. D. Bender, "An inter-system handoff technique for the IMT-2000 system," in *Proc. INFOCOM*, 2000, pp. 208–216.
[32] A. Mishra, M. Shin, and W. Arbaugh, "An empirical analysis of the IEEE 802.11 MAC layer handoff process," *ACM SIGCOMM Comp. Commun. Rev.*, vol. 33, no. 2, pp.93–102, Apr. 2003.
[33] J. McNair, I. F. Akyildiz, and M. D. Bender, "Handoffs for real-time traffic in mobile IP version 6 networks," in *Proc. IEEE GLOBECOM*, 2001, pp. 3463–3467.

Seonggeun Ryu received his B.S. degree in Computer Science from Yonsei University, Korea in 2002 and M.S. and Ph.D. degrees in School of Computing from Soongsil University, Korea in 2006 and 2011, respectively. Currently, he is a Postdoctoral Researcher at Daegu Gyeongbuk Institute of Science and Technology (DGIST), Korea. His research interests include analyzing, modeling, improving, and securing IP-based mobility management protocols for next-generation wireless mobile networks and vehicular networks.

Ji-Woong Choi received the B.S., M.S., and Ph.D. degrees in Electrical Engineering from Seoul National University (SNU), Korea in 1998, 2000, and 2004, respectively. From 2004 to 2005, he worked as a Postdoctor in Inter-University Semiconductor Center (ISRC), SNU, Korea. From 2005 to 2007, he was with the Department of Electrical Engineering, Stanford University, Stanford, CA as a Postdoctoral Visiting Scholar. He also worked as a Consultant in GCT Semiconductor, San Jose, CA for development of mobile TV receivers from 2006 to 2007. From 2007 to Oct. 2010, he worked for Marvell Semiconductor, Santa Clara, CA as a Staff Systems Engineer for next generation wireless communication systems including WiMAX and LTE. Since Oct. 2010, he has been with the Department of Information and Communication Engineering, Daegu Gyeongbuk Institute of Science and Technology (DGIST), Daegu, Korea as an Assistant Professor. His research areas are wireless communication theory, signal processing, bio-medical communication applications, and brain machine interface. He received Silver Award at Samsung Humantech Paper Contest in Feb. 2005 and IT National Scholarship from the Ministry of Information and Communication, Korea in Oct. 2005.

Kyung-Joon Park received his B.S. and M.S. degrees from the School of Electrical Engineering and Ph.D. degree from the School of Electrical Engineering and Computer Science, Seoul National University, Seoul, Korea. He is currently an Assistant Professor in the Department of Information and Communication Engineering, Daegu Gyeongbuk Institute of Science and Technology (DGIST), Daegu, Korea. He was a Postdoctoral Research Associate in the Department of Computer Science, University of Illinois at Urbana-Champaign (UIUC), IL, USA from 2006 to 2010. He was with Samsung Electronics, Suwon, Korea as a Senior Engineer, from 2005 to 2006, and was a Visiting Graduate Student in the Department of Electrical and Computer Engineering, UIUC in 2001 and 2002. His current research interests include modeling and analysis of cyber-physical systems and design of medical-grade protocols for wireless healthcare systems. He is currently serving on the editorial boards of Wiley Transactions on Emerging Telecommunications Technologies. He has served as Lead Guest Editor for the special issue on cyber-physical systems in Computer Communications. He has also served as a Program Committee Member of numerous international conferences on wireless networking. He is a recipient of the Gold Prize in the Samsung InsideEdge Thesis Competition.